

RESEARCH ARTICLE

Ventilation-induced epithelial injury drives biological onset of lung trauma in vitro and is mitigated with prophylactic anti-inflammatory therapeutics

Eliram Nof¹  | Arbel Artzy-Schnirman¹  | Saurabh Bhardwaj¹  |
 Hadas Sabatan¹ | Dan Waisman^{2,3}  | Ori Hochwald^{2,4}  | Maayan Gruber^{5,6} |
 Liron Borenstein-Levin^{2,4}  | Josué Sznitman¹ 

¹Faculty of Biomedical Engineering, Technion - Israel Institute of Technology, Haifa, Israel

²Faculty of Medicine, Technion - Israel Institute of Technology, Haifa, Israel

³Department of Neonatology, Carmel Medical Center, Haifa, Israel

⁴Department of Neonatology, Ruth Rappaport Children's Hospital, Rambam Healthcare, Haifa, Israel

⁵Azrieli Faculty of Medicine, Bar-Ilan University, Safed, Israel

⁶Department of Otolaryngology-Head and Neck Surgery, Galilee Medical Center, Nahariya, Israel

Correspondence

Josué Sznitman, Faculty of Biomedical Engineering, Technion - Israel Institute of Technology, Haifa 3200003, Israel.
 Email: sznitman@bm.technion.ac.il

Funding information

European Research Council (ERC) under the European Union's Horizon 2020 research and innovation program, Grant/Award Number: 677772

Abstract

Mortality rates among patients suffering from acute respiratory failure remain perplexingly high despite the maintenance of blood oxygen homeostasis during ventilatory support. The biotrauma hypothesis advocates that mechanical forces from invasive ventilation trigger immunological mediators that spread systemically. Yet, how these forces elicit an immune response remains unclear. Here, a biomimetic in vitro three-dimensional (3D) upper airways model allows to recapitulate lung injury and immune responses induced during invasive mechanical ventilation in neonates. Under such ventilatory support, flow-induced stresses injure the bronchial epithelium of the intubated airways model and directly modulate epithelial cell inflammatory cytokine secretion associated with pulmonary injury. Fluorescence microscopy and biochemical analyses reveal site-specific susceptibility to epithelial erosion in airways from jet-flow impaction and are linked to increases in cell apoptosis and modulated secretions of cytokines IL-6, -8, and -10. In an effort to mitigate the onset of biotrauma, prophylactic pharmacological treatment with Montelukast, a leukotriene receptor antagonist, reduces apoptosis and pro-inflammatory signaling during invasive ventilation of the in vitro model. This 3D airway platform points to a previously overlooked origin of lung injury and showcases translational opportunities in preclinical pulmonary research toward protective therapies and improved protocols for patient care.

KEY WORDS

drug testing, epithelial cells, inflammation, lung, preclinical in vitro model, respiratory distress, ventilation

1 | INTRODUCTION

Acute respiratory failure epitomizes a deleterious lung condition associated with high mortality rates (>35%) in critical care patients undergoing ventilatory support,¹ despite the maintenance of blood oxygen

homeostasis.^{2,3} In deciphering this conundrum, the pulmonary biotrauma theory suggests a multifactorial cascade, starting with invasive mechanical forces triggering the release of immunological mediators in the lungs.⁴ Cyclic respiratory airflows are hypothesized to facilitate the distribution of such mediators and their translocation

This is an open access article under the terms of the Creative Commons Attribution License, which permits use, distribution and reproduction in any medium, provided the original work is properly cited.

© 2021 The Authors. *Bioengineering & Translational Medicine* published by Wiley Periodicals LLC on behalf of American Institute of Chemical Engineers.

across the alveolar-capillary barrier into the wider systemic circulation.³ In turn, inflammatory effects may spread and amplify throughout the body leading to multi-organ failure and eventually death.³

Biotrauma was first proposed in the context of invasive mechanical ventilation; a life-supporting clinical intervention also recognized to concurrently cause or worsen lung morbidity.² Most recently, mechanical ventilation has gained increased scrutiny amidst the COVID-19 pandemic,^{5–7} owing to alarmingly higher mortality rates among patients requiring respiratory support^{8,9} (~50%–97%). The main physical mechanisms identified as contributing to pulmonary injury¹⁰ include the overstretching during ventilation of lung tissue from over inflation (known as volu- or barotrauma) and the repeated opening and collapse of small airway units at excessively low volumes (i.e., atelectrauma). Various protective ventilation protocols have emerged to marginally improve patient outcomes and reduce mortality.¹¹ Yet eliminating injurious mechanical forces is elusive as underlined in clinical trials.¹² Recent efforts have begun exploring therapeutic opportunities (e.g. gene delivery) to mitigate lung injury in the deep alveolar regions.¹³ Still, it remains widely unknown to what extent mechanical forces influence the downstream precursors leading to biotrauma. Indirect evidence from animal models^{14,15} and clinical studies^{11,16} has provided seminal support for the biotrauma hypothesis. However, a direct corroboration *in vivo* is challenging since lung-derived inflammatory biomarkers in patients are not readily collected in clinical settings in detecting the origins of cytokine release and trafficking.¹⁷

In an effort toward bridging this gap, engineered *in vitro* lung models leveraging advances in tissue engineering and microfabrication have been increasingly utilized for advancing preclinical pulmonary research and explore lung injury.^{18,19} For example, *in vitro* studies have characterized wounding in alveolar epithelial cells subjected to cyclic overstretching, including the release of inflammatory cytokines, impaired structural integrity via changes in tight junctions and plasma membrane breaks, and increased incidence of apoptosis.^{20–22} Cellularized *in vitro* models have typically focused on the airway epithelial barrier of the deep acinar regions,²³ where mechanical stresses are dominated by tensile strains when the alveolar airway barrier expands and contracts cyclically.²⁴ In contrast, there has been little emphasis on the lungs' proximal regions (i.e., upper airways), where airflow dynamics are most prominent. Namely, the exposure of bronchial epithelial cells to respiratory flow-induced shear stresses has been proposed as a potential link between large ventilation pressures and morbidity and mortality²⁵; a situation strongly correlated in ventilated patients undergoing surgery in the absence of prior lung injury.²⁶ In support, computational fluid dynamics (CFD)-based *in silico* studies have found that upper airway flow phenomena and ensuing wall shear stresses (WSS) may contribute to ventilator-induced lung injury (VILI) via the biotraumatic pathway.^{27–29} We have also recently underlined the plausible occurrence of such injury during invasive endotracheal intubation maneuvers.³⁰ Nevertheless, *in silico* studies are limited in addressing inflammatory cascades arising in conducting airways and have instead relied on extrapolation from hemodynamic studies with endothelial cells, limiting their clinical relevance.³¹

In the present work, we explore for the first time the hypothesis of potential immunological mediators originating in the upper respiratory tract of preterm infants as a result of ventilatory flow-induced shear stresses. Preterm infants are particularly susceptible to VILI as a result of potentially extended periods of ventilatory support.³² To this end, we developed a true-scale, three-dimensional (3D) bronchial epithelial airway *in vitro* model of the tracheobronchial tree subject to physiologically realistic ventilatory protocols in intubated pediatric populations that are prone to VILI.³² We expose injurious effects of flow-induced WSS on the epithelial airway barrier populating the 3D airway lumen, leveraging phenotypical endpoints of epithelial structural integrity, cell apoptosis, and importantly the secretion of cytokines associated with inflammatory pathways. Our *in vitro* assays support the manifestation of shear flow-induced lung injury during mechanical ventilation, thus strengthening the biotrauma hypothesis. Furthermore, our findings may help associate rare but acute adverse effects (e.g. necrotizing bronchitis, epithelial erosion, and loss of surface cilia) observed in clinical³³ and animal³⁴ studies on ventilation associated injury. To mitigate the initiation of such inflammatory cascades during ventilation, we demonstrate as a proof-of-concept the topical delivery of a widely used anti-inflammatory respiratory therapeutic as a prophylactic strategy for preventive action that supports opportunities in preclinical pulmonary research toward protective therapies.

2 | RESULTS

2.1 | Development of 3D bronchial epithelial airway model

As preterm infants are a unique patient population that may exhibit significant damage resulting from mechanical ventilation support,³² we engineered an *in vitro* neonatal upper airway model (Figure 1a) to investigate the effects of flow-induced shear stresses on the tracheobronchial epithelium during intubated ventilation. The model spans the trachea to the first three bronchial generations of the airway tree (Figure 1b) and adheres closely to the idealized planar double-bifurcating Weibel³⁵ lung model.^{36,37} Following previously reported methods,^{30,38} we homothetically scaled the model's geometric dimensions to the anatomical size of a ~2 kg (~33 weeks old) preterm infant based on the tracheal diameter. We used additive manufacturing (i.e., 3D printing) to fabricate a cast (Figure 1c) and filled it with liquid polydimethylsiloxane (PDMS). Following polymerization, we dissolved the printed material leaving a transparent PDMS phantom (Figure 1d) used as an anatomically realistic scaffold architecture for cell culture. Next, extracellular matrix (ECM) proteins (fibronectin and collagen) were used to coat the model's inner surface before cell culture following an optimized coating study (see Figures S1 and S2). Here, we cultured Calu-3 cells (Figure 1e); Calu-3 is an established human bronchial epithelial cell line and widely used in preclinical pulmonary research for drug screening and toxicity,^{39,40} thereby recapitulating a relevant epithelium lining the bronchial regions. Specifically,

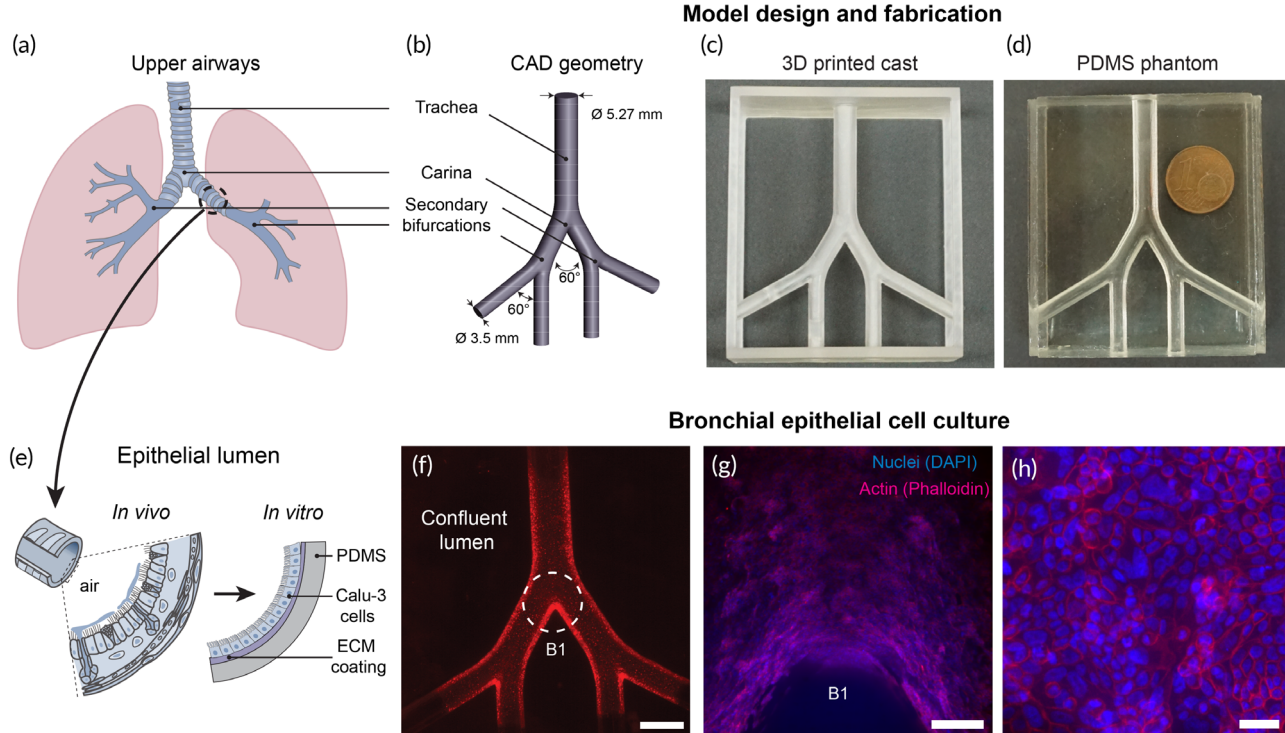


FIGURE 1 Development of a true-scale, three-dimensional (3D) bronchial epithelial airway model. (a) Schematic of the lungs including the conducting upper airways. (b) Computer-aided design (CAD) of a simplified, symmetric, double-bifurcating model starting at the first generation of the airway tree (i.e., trachea) up until and including the third bifurcating generation of bronchi. The model's dimensions match the scale of a ~33-week old (preterm) infant. (c) 3D-printed cast used to fabricate a (d) transparent, polydimethylsiloxane (PDMS) phantom photographed alongside one euro (€) cent coin for scale. (e) The in vivo epithelium-lined lumen is recapitulated in vitro by culturing bronchial Calu-3 cells on the PDMS surface coated with extracellular matrix (ECM) materials (i.e., fibronectin and collagen). (f) The model is imaged via stereomicroscope and red fluorescent membranal staining (CellTracker Red CMTPX), exhibiting a fully confluent monolayer of cells covering the inner lumen surface. Scale bar in (f) is 5 mm. A dashed white circle highlights the first bifurcation (tracheal carina), shown at two magnifications: (g) 4× and (h) 20× after staining F-actin (Phalloidin-iFluor 555) and nuclei (DAPI). Scale bars for (g) and (h) are 200 and 40 μ m, respectively. See Section 4 for more details on fabrication and cell culture

using an airway epithelial cell line permits experimental control and reproducibility as a preclinical benchmark by reducing variability in cell cultures arising from donor-to-donor differences⁴¹ while maintaining key features of the bronchial epithelium in human lungs (e.g., tight junctions, mucus secretion, cytokine production and more).

Models were cultured under immersed conditions and tracked over 3–4 weeks until a fully confluent epithelial monolayer populated the entire 3D airway lumen (Figure 1f). As recently shown in silico, jet-flow impaction in airways can be significant during invasive mechanical ventilation.³⁰ Hence, monitoring cell structural integrity is critical (see tight junction occluding protein staining in Figure S2), in particular, at the bifurcations (e.g., main carina in Figure 1f–h). Our development of more realistic 3D in vitro airway morphologies is supported by recent studies where Calu-3 cells (as well as other epithelial cells) cultured on curved membranes and inside lumen exhibit distinct characteristics from traditional two-dimensional monolayers, including cell density and shape, apoptotic ratios, and cross-sectional morphology.^{42,43} Here, we specifically designed a planar bifurcating geometry to facilitate microscopy imaging by limiting the model's vertical dimension, whose 3D curvature of the inner lumen extends

outside the depth of focus under higher magnifications (Figure 1h). The total volume enclosed within the model is 1.5 ml, efficiently and robustly removed or exchanged via plastic connector ports inserted into all outlets for model maintenance, allowing for the simple removal of medium and cell collection for further analysis such as ELISA and flow cytometry (see below).

2.2 | In vitro and in silico flow dynamics reveal focal shear stresses under invasive mechanical ventilation

The intricate flow patterns in the human respiratory airways are mainly driven by the interaction of time-dependent flow fields in the upper airway generations (starting in the trachea) with changing geometries, including changes in cross-sectional areas, wall curvatures, and carinal edges across the airway tree.³⁶ We studied both in experiments and simulations the flow dynamics in our model by imposing symmetric, sinusoidal flowrate profiles (Figure 2a) at the model's inlet mimicking the inhalation and exhalation phases under

intubated, positive pressure ventilation conditions that are fundamentally distinct from normal physiological ventilation under negative pressure conditions. We note that modern ventilators, including those used in our simulated clinical settings (see Section 2.3), use more complex (i.e., asymmetric inspiratory/expiratory rates) ventilation profiles. These adapt in real-time to patient breathing conditions and are set using pressure-based values. Here, ventilatory airflows are driven into the *in vitro* upper airway model by setting velocity-based boundary conditions at the inlet extracted from clinically relevant tidal volumes and breathing rates following previously reported methods^{30,38} (see Section 4).

Transient, temporally resolved 3D velocity vector fields were measured via tomographic particle image velocimetry³⁰ (TPIV) (Figure 2b-c). A nearly identical PDMS phantom model (Figure S3) was substituted to specifically improve optical access (with the addition of transparent side windows) and robustness (i.e., nylon tube connector in place of the endotracheal tube, ETT, of comparable inner diameter, ID). For the TPIV setup (see Figure S3), four cameras at specifically offset angles were used to simultaneously image the flow in the model, fully capturing 3D flow features. Further processing involves triangulating the location of flow-tracing particles in a volume between the multiple cameras to resolve the flow in 3D space (see Section 4). Analysis of the extracted flow fields reveals that a flow jet exiting the ETT and impacting on the main carina is the most dominant flow feature in the intubated upper airways, in particular at peak strength midway during the inhalation phase (Figure 2a), and supporting recent findings in a study using a six-generation intubated neonatal upper airway model.³⁰

We next ran *in silico* CFD simulations modeling identical flow conditions in the airway model over several ventilation flow profiles using the finite-volume method (FVM) and compared results with experimental measurements for validation. In Figure 2d, we plot a numerical solution matching the experimental case conditions shown in Figure 2c, with orthogonal cut planes colored according to the normalized velocity magnitudes and an overlay of velocity vectors. Given the spatial imaging limitations in TPIV experiments,³⁰ CFD is particularly useful in resolving flows at higher spatial resolution, in particular at the carina and in the vicinity of the lumen walls. In Figure 2e, we plot the computed WSS on the model lumen during peak inspiration when the inhalation jet is at peak strength. We find an elevated WSS region localized at the jet's impaction site with the main carina, shown in an enlarged inner side view in Figure 2f. Here, local WSS values exceed 1500 dyn cm^{-2} ; namely two orders of magnitude higher than levels found to impair epithelial permeability in human and mice bronchial epithelial cells.⁴⁴ We find lower ($<300 \text{ dyn cm}^{-2}$) WSS values concentrated in the two daughter bifurcations, an $\sim 80\%$ attenuation relative to the first generation due to viscous energy dissipation and anticipated to occur in any symmetrically branching channel system.⁴⁵ We performed four additional simulations with smaller tidal volumes but identical flow rates (i.e., breathing frequency is increased according to the linear relationship $Q = f \times TV$, where Q is the flow rate, f the frequency, and TV the tidal volume³⁰) and tracked the peak WSS values at the main carina. In Figure 2g, results are plotted as a

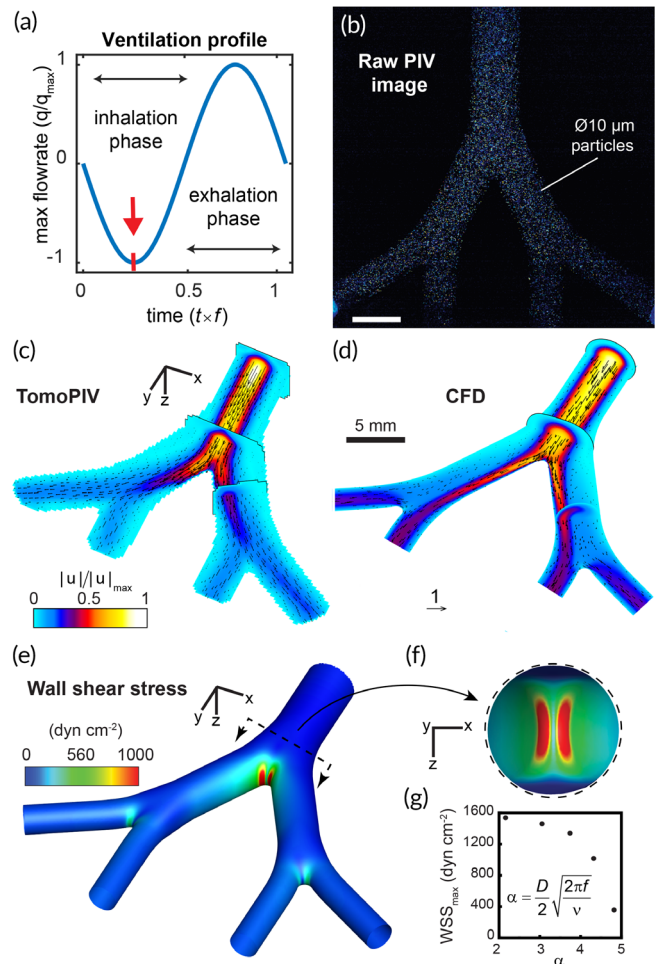


FIGURE 2 In vitro and *in silico* fluid dynamics analysis reveals a region of elevated shear stress concentrated at the tracheal carina during the inspiratory phase of intubated ventilation in a neonatal-sized airway model. (a) A sinusoidal flow profile mimicking oscillatory mechanical ventilation is imposed on the model via perfusion at the inlet (trachea). The first quarter of the cycle (see red arrow) marks the inspiratory phase's peak strength when air is pushed into the model. The flow is visualized and measured experimentally using tomographic particle image velocimetry (TPIV), demonstrated with a raw image (b) from one of four cameras in the TPIV setup (see Section 4 and Figures S3 and S4), showing illumination of $10 \mu\text{m}$ diameter fluorescent particles captured instantaneously while tracing the streamlines of the flow. Following image analysis (i.e., image pre-processing and TPIV algorithms), the three-dimensional transient flow is fully resolved. The flow field at peak inspiration is plotted in (c), with several orthogonal cut planes colored by the normalized velocity magnitude contour field and overlaid with velocity vectors. (d) An *in silico*, that is, computational fluid dynamics (CFD), solution is compared with the experimental data. During peak inspiration, the most dominant flow feature is captured by a synthetic jet exiting the endotracheal tube and impacting the first carina. A numerical solution allows for finer near-wall resolution and analysis of WSS, mapped by colored contours in (e) with a top view of the first bifurcation shown in the inset (f). Panels (b)–(f) feature a flow analysis of a representative low-frequency ventilation protocol most similar to conventional mechanical ventilation used in cellular *in vitro* experiments. In (g), maximum WSS levels measured at the first bifurcation are plotted as a function of normalized ventilation frequency, or α (i.e. Womersley number), for five ventilation protocols solved using CFD (see Figure S5)

function of the Womersley number, a nondimensional frequency number defined as $\alpha = D/2\sqrt{2\pi f/\nu}$, where D is the airway diameter and ν the kinematic viscosity. A reduction in maximum WSS values relative to α (varied between 2 and 5) indicates that lower tidal volumes at higher frequencies attenuate the flow jet's effects, implying a possible link to the acknowledged protective benefits of low tidal volume ventilation.⁴⁶ We note that negative pressure ventilation,⁴⁷ an alternative ventilatory support technique that drives gas flow into the lungs by reducing pressure around the patient's chest and thus more closely mimics normal physiological breathing, is fundamentally different from intubated, positive pressure driven ventilation described here and is thus anticipated to give rise to different WSS distributions that would resemble more closely normal breathing features.

We next compare these findings to previous numerical studies on flow-induced shear stress in human airways and find similarly reported patterns of local peaks at the bifurcating sites.⁴⁸ In an airway model of generations 3–5, elevated WSS ($\sim 5 \text{ dyn cm}^{-2}$) were reported localized at the bifurcations,⁴⁹ matching our findings that the primary site for WSS is indeed at the impaction site of the intubation jet with the main carina and that subsequent bifurcations witness the localization of far lower shear stresses. A large eddy simulation type computational study found that the addition of an ETT in a computed tomography (CT) scan patient-derived airway model increased WSS at the main carina during inspiration by $\sim 87\%$ to a peak of $\sim 200 \text{ dyn cm}^{-2}$. These values are likely lower than our peak WSS values as their study focused on high-frequency ventilation protocols ($10 < \alpha < 20$) using smaller tidal volumes. Furthermore, our study uniquely focuses on a smaller, neonatal-sized airway geometry under pediatric ventilation conditions, which we anticipate to increase local airflow velocity and WSS values relative to corresponding adult settings, as discussed in a recent age-comparative respiratory study.⁵⁰ Our flow analysis corresponds to an ETT positioned axisymmetrically in the trachea of our transparent model. In clinical practice, medical imaging (e.g., X-ray) is required to confirm proper ETT placement; a situation that may be altered by the infant's movement and changes in body position. Muller et al.⁵¹ studied the effects of ETT positioning on tracheal WSS under high-frequency jet ventilation (HFJV), concluding that shear forces were amplified more than twice in cases where ETT tubes were placed asymmetrically more proximal to the tracheal wall, indicating our relatively conservative approach for the ETT placement.

2.3 | Replicating clinical settings of invasive ventilation *in vitro*

Once models achieved full epithelial confluence following 3–4 weeks of culture (Figure 3a), these were prepared for exposure to invasive ventilation, replicated with equipment and corresponding clinical settings typically used in neonatal intensive care units, as described schematically in Figure 3b,c. A 3.0 mm ID uncuffed ETT was inserted 2 cm above the first bifurcation apex (see enlarged inset in Figure 3b), matching approximately the insertion depth of 8 cm for a 2 kg (~ 33 weeks) infant following the American Academy of Pediatrics

guidelines.³² Clinical ventilation settings were maintained (in the absence of the lower regions of the lung) by fitting compliance adapters (small latex balloons, see Figure 3b) to the four outlets of the model and calibrated to match clinical pressure and lung compliance conditions monitored by the ventilator (see Figure 3c and Section 4). A natural rubber latex membrane was similarly used and calibrated in simulating lung compliance of distal airways *in vitro* in a study on the role of ventilation mechanics in reopening a collapsed lung.⁵² As a control for the ventilation exposure assay, an additional upper airway model was placed alongside and connected to identical tubing and compliance adapters in the absence of any airflow ventilation. To explore ventilation conditions on the epithelium at the air–liquid interface (ALI), models were emptied of culture medium (stored for cytokine analysis, see below), connected to ventilation tubing, and ventilated for 4 h. Models were kept inside an incubator (37°C , 5% CO₂) for the duration of the exposure to factor for environmental stress not associated with the ventilation (see Figure 3c,d). Ventilator settings (Table 1) were chosen on the higher side of the recommended clinical range, used for infants with significant breathing difficulty and at a low respiratory rate^{53,54} (i.e., frequency). These settings were selected to underline the potential for damage, following our flow analysis revealing the effects of shear stresses under intubated ventilation conditions, and highest at lower respiratory frequencies. Following the 4-h exposure assay, models were refilled with fresh cultured medium and returned to the incubator. Later, this medium was collected at identical culture time intervals as pre-exposure samples.

In line with our experimental flow analysis identifying localized, elevated WSS sites (Figure 2), we found evidence of physical damage to the epithelium in our model at the same locations following exposure to intubated ventilation conditions. Epithelial erosion (i.e., the detachment of epithelial cells from the model) was observed using fluorescent nuclei staining (Figure 3e) at the first bifurcation (i.e., main carina) 48 h following a simulated ventilation exposure. We tracked the evolution of epithelial erosion by imaging in bright-field the live cells in the models at several time points following ventilation and compared it to the initial pre-ventilation image at the same locations (see Figure S6). Erosion was not observed in other regions of the ventilated model, including the two daughter bifurcations where minor shear stress localization was predicted by the flow analysis (Figure 2e). Notably, epithelial erosion in the tracheobronchial region is known as a severe histopathological marker of inflammation and acute lung injury found in pathological slides sampled from infants who died following mechanical ventilation.^{33,55} The prevalence of this damage in invasively ventilated infants today is mostly unknown due to lower mortality rates and autopsy protocols that may not include specific microscopic examinations of the trachea, carina, or mainstem bronchi. Moreover, epithelial restoration mechanisms⁵⁶ may repair denuded regions in surviving infants, further obscuring potential observation of this phenomena in the clinic. Solid mechanical stresses in the context of cyclic reopening were shown to contribute to alveolar epithelial cell death and detachment in a microfluidic model⁵⁷ and may similarly be a suitable proxy here for identifying structural lung pathology *in vitro*.

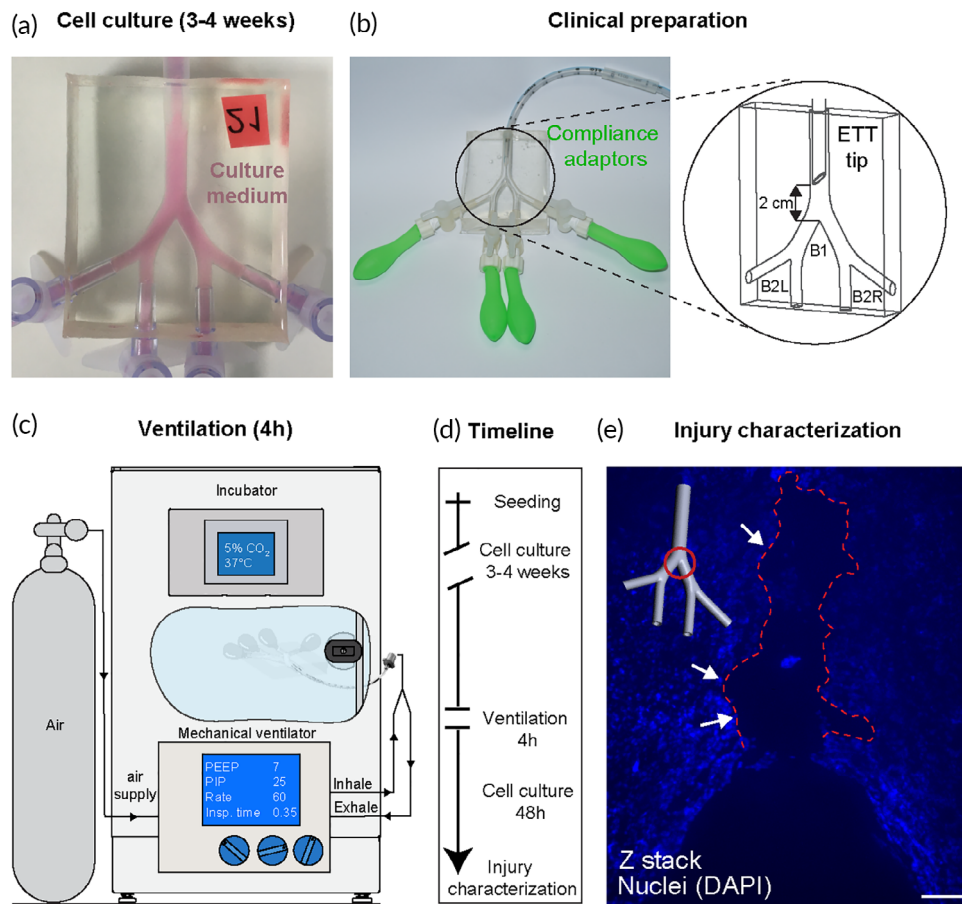


FIGURE 3 Simulated mechanical ventilation experimental setup and detection of cellular injury. (a) The three-dimensional lumen epithelium is recapitulated by seeding bronchial cells (Calu-3) inside the model and cultured at 37°C and 5% CO₂ until full confluence is achieved (3–4 weeks). Before exposure to either ventilation or control conditions, models are imaged, and their culture medium collected for subsequent cytokines analysis, serving as a reference point for a priori conditions. (b) Next, the model is prepared for clinical ventilation by installing compliance adapters (latex balloons) at the four outlets (to simulate pressure conditions present in a full lung) and inserting a 3.0 mm ID uncuffed endotracheal tube (ETT) 2 cm above the first carina (marked B1), following clinical guidelines for proper insertion depth. The two daughter branches are marked B2L (left) and B2R (right) following anatomical orientation convention. Note that during ventilation, the ETT tip is placed symmetrically while here shown at a 90° rotation for clarity. (c) Models are ventilated inside the incubator with medical-grade air, supplied via a breathing circuit connected to a neonatal mechanical ventilator for 4 h using settings defined in Table 1. After the exposure, models are filled with medium and returned to the incubator for an additional 24–48 h before further analysis and injury characterization, including microscopy imaging. (d) Timeline of experimental protocol and endpoints. (e) Fluorescent bright-field microscopy imaging reveals a region of cell detachment localized at the first bifurcation, exhibited 48 h following invasive ventilation. Scale bar is 100 μm. The delayed onset of epithelial erosion, that is, a severe form of cell injury, demonstrates the complex traumatic pathway following exposure to flow-induced shear stresses during invasive ventilation. Regions of cell detachment are highlighted with red dashed line

2.4 | An increase in cell apoptosis indicates an early biotrauma cascade

Following ventilation/control exposure experiments, cells were harvested from the models and analyzed for cell death using fluorescence-activated cell sorting (FACS) with apoptosis/necrosis using Annexin-V/propidium iodide (PI) staining (Figure 4a–c). Annexin-V provides a sensitive method for detecting cellular apoptosis, while PI is used to detect necrotic or late apoptotic cells. Nearly all cells from the control models (i.e., zero flow conditions) were found to be viable cells (double-negative) when analyzed at both 24- and 48-h time points following exposure (Figure 4a), while large decreases in %

live cells were found among the ventilated models. The % population of live cells (indicated double-negative for both Annexin-V and PI) in ventilated models decreased by 60% with 24 h following the exposure and 75% at 48 h, respectively. Most nonviable cells were found in the apoptotic subpopulation (indicated double-positive for both Annexin-V and PI), increasing from <5% of the total cell population to 55% and 60% at 24 and 48 h, respectively. Necrotic cells (indicated positive for PI and negative for Annexin-V) were found in negligible levels in both control and ventilated models at both time intervals, as seen in Figure 4c. We note here that cell detachment observed in a small region near the carina at 48 h following ventilation exposure (see Figure 3e) may introduce a bias to the 48-h postexposure

TABLE 1 Mechanical ventilator settings used during in vitro cell-based experiments on neonatal-sized upper airway models are presented. Flow conditions are set using pressure- and time-based parameters following clinical convention. An infant-pediatric ventilator (see Figure 3c) was enlisted to provide realistic clinical ventilation conditions typically used in the Neonatal Intensive Care Unit (NICU). These values lie on the higher side of the recommended clinical range, used for infants with significant breathing difficulty and at a low respiratory rate. In contrast to the simplified flow profiles (see Figure 2a), modern ventilators feature advanced control modalities that produce more complex flow cycles

| Parameter | Value | Units |
|----------------------------------|-------|--------------------|
| Positive end-expiratory pressure | 7–8 | cmH ₂ O |
| Peak inspiratory pressure | 25 | cmH ₂ O |
| Respiratory rate | 60 | bpm |
| Inspiratory time | 0.35 | s |

analysis, although we anticipate this effect to be negligible owing to the small (<1%) surface area affected relative to the total luminal area of the model. In interpreting such results, we recall that cell apoptosis is a tightly regulated mechanism routinely employed in maintaining normal tissue and organ homeostasis. Macrophages remove apoptotic cells through phagocytosis, a process enhanced via the local release of anti-inflammatory cytokines interleukin IL-10 and TGF- β 1 by both macrophages and apoptotic cells.⁵⁸ Incidence rates of apoptosis among airway epithelial cells above normal levels can indicate a compensatory response to disease or a pathogenetic consequence, or both.⁵⁹ Pulmonary inflammation and fibrosis are known to be linked to the accumulation of excessive apoptotic cells or the cleavage of cell remnants, which in turn may promote further inflammatory processes.⁵⁸

2.5 | Ventilation exposure modulates epithelial inflammatory cytokine secretions

To explore the causal relationship between biophysical injury and induced inflammatory response, the central tenet to the biotrauma hypothesis,³ we tracked the secretion of cytokines known to be critical mediators of pulmonary injury and inflammation. Secreted concentrations of pro-inflammatory (IL-6, IL-8) and suppressive anti-inflammatory (IL-10) cytokines were measured in the sampled cultured medium at two intervals: 24 and 48 h before and after the ventilation/control exposure. In Figure 4d-f, cytokine secretions are plotted as fold change relative to baseline, pre-exposure levels. As an immortalized cell line, Calu-3 exhibit basal levels of cytokine secretion that depend highly on cell passage,⁶⁰ therefore calculating the difference in cytokine production between exposure states filters this bias and allows for batch model interpretation. We found decreased IL-6 and IL-8 among the ventilated models at both time intervals, while the control group showed slightly increased levels. At 24 and 48 h, IL-6 decreased by more than half of baseline levels and ~75% relative to the control; IL-8 decreased ~25% at 24 h and 50% relative to the

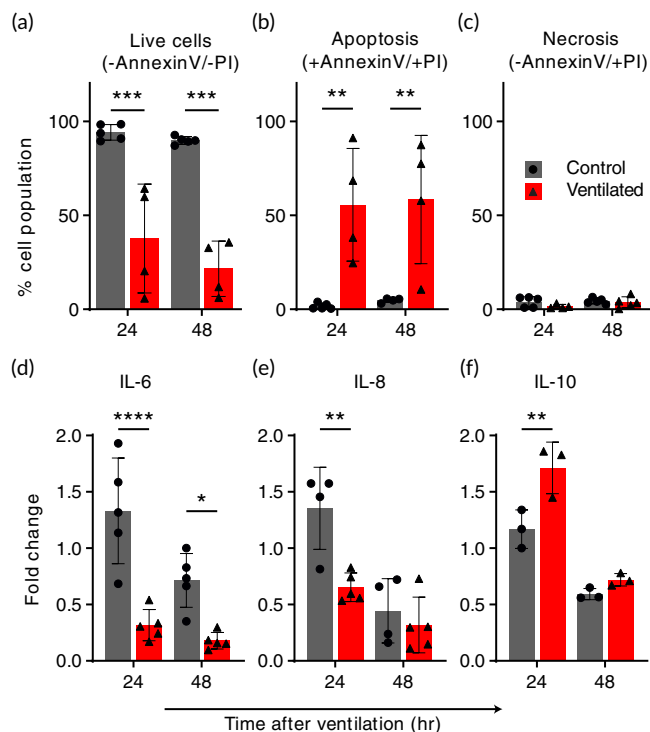


FIGURE 4 Ventilation exposure modulates apoptotic pathways and epithelial inflammatory cytokine secretions. Cells and culture medium were collected from models 24 and 48 h following ventilation exposure and compared with baseline levels. Air ventilation was performed for 4 h, or the ventilator machine kept off for the same duration as a control. Following the exposure, culture medium was filled back into the models. (a-c) An increase in apoptotic cells indicates a biotraumatic response. Cells were collected from models and analyzed using flow cytometry (FACS) following Annexin-V and Propidium Iodide (PI) staining. The % total population of (a) live cells decreased by 60% at 24 h and 75% at 48 h in the ventilated group relative to the control, which is largely unaffected at either time point. Most of this increase in nonviable cells is found in (b) the apoptotic, ventilated group while (c) negligible necrotic cells were counted for either exposure group. The increase in apoptosis was consistent in models analyzed both 24 and 48 h following the exposure experiment. (d-f) Changes in the secretion of inflammatory cytokines following ventilation suggest a signaling pathway. Cytokines IL-6 (d), IL-8 (e), and IL-10 (f) were measured in culture medium collected from the models after 24 and 48 h periods before and following simulated ventilation, respectively. Measurements from repeated experiments are plotted as normalized fold change to highlight signaling changes resulting from the test exposure. In (d) and (e), we measured a significant reduction in pro-inflammatory IL-6 (75% at both 24 and 48 h) and IL-8 (50% at 24 h) relative to the control, while conversely in (f), we find that IL-10, an anti-inflammatory cytokine, is elevated >30% at the 24-h time point compared with the control. All values are normalized relative to their baseline, that is, divided by pre-exposure secretory levels. Cytokines were measured using ELISA. All graphs show mean (SD) values. * $p < 0.05$; ** $p < 0.01$; *** $p < 0.001$; **** $p < 0.0001$

control group, with no statistically significant reduction at 48 h. Conversely, elevated concentrations of IL-10 were measured 24 h after ventilation while the control remained close to baseline levels. All

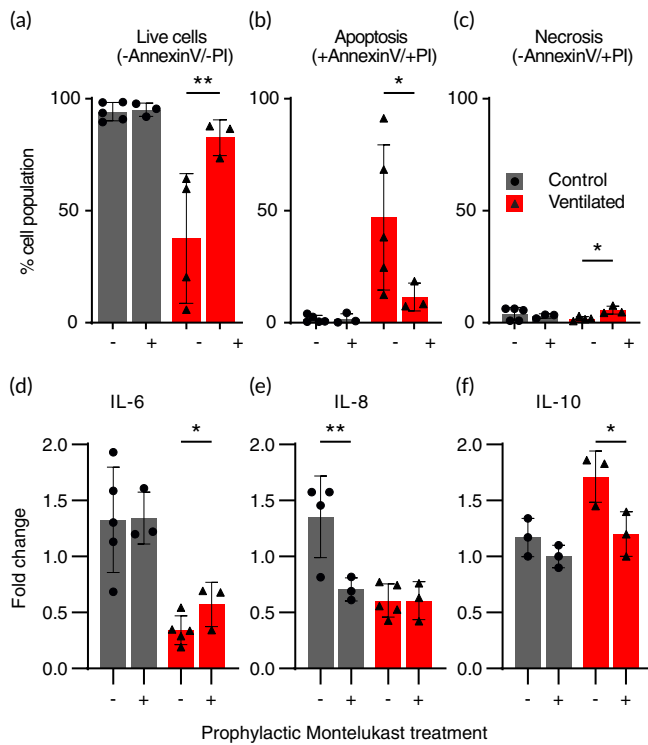


FIGURE 5 A prophylactic leukotriene receptor antagonist (Montelukast) reduces cell apoptosis and modulates inflammatory cytokine secretion in bronchial epithelial airway models exposed to ventilation injury. Montelukast, an asthma anti-inflammatory medication commonly used to treat pulmonary asthma, was supplemented in the culture medium of models for 2 h before ventilation exposure. Flow cytometry was performed on cells collected from models 24 h following the ventilation/control and stained with Annexin-V and Propidium Iodide (PI), indicating % of the cell population (a) live, (b) apoptotic (c), or necrotic. Montelukast pretreatment significantly increased (55%) the number of live cells in the ventilated group by reducing apoptosis (75%) while showing no adverse impact on the control group's high live cell count. (c) An increase in necrotic cells (70%) was observed in the ventilated group while absent in control, with a negligible effect on %total of live cells due to low overall counts (maximum of 5% total population). (d-f) Cytokine secretions were measured in the culture medium collected from all models 24 h after the ventilation exposure. Cytokines IL-6 (d), IL-8 (e), and IL-10 (f) are plotted as fold change normalization to highlight changes in signaling resulting from the test exposure. (d) We report no significant difference in IL-6 secretion in the control groups, while an increase in IL-6 secretion (67%) was measured in the pre-treated ventilated group relative to nontreated. (e) In contrast to IL-6, IL-8 secretion was found reduced in the control group (50%) following prophylactic treatment, while we measured no difference due to treatment in the ventilated groups. Lastly, we measured the suppressory IL-10 secretion, with mean values unaltered in the control groups but reduced by 30% following prophylactic treatment with Montelukast. All cytokine secretion values are plotted as fold change, i.e., normalized relative to their baseline pre-exposure levels. Cytokines were measured using ELISA. All graphs show mean (SD) values. * $p < 0.05$; ** $p < 0.01$; *** $p < 0.001$; **** $p < 0.0001$

cytokine secretory events were observed to be most prominent in the first 24 h following the exposure, while at 48 h effects were found diminished, indicating the transitory nature of the response to a single,

4-h ventilation exposure protocol. Notably, IL-10 is known to play a crucial role in regulating immune responses by limiting and ultimately terminating inflammatory events via the inhibition of cytokine synthesis.⁶¹ One possible explanation for our findings is that at 24-h post-stimulus, pro-inflammatory cytokine production is inhibited by IL-10 due to an anti-inflammatory response.

2.6 | Prophylactic leukotriene receptor antagonist reduces cell death and modulates the secretion of inflammatory cytokines

After establishing the presence of an inflammatory response to flow-induced shear stress in our model (Figure 4), we next sought a direct modulatory agent that could demonstrate the model's application for therapeutic preclinical research. As a proof-of-concept, we tested the prophylactic effect of the commonly used airway anti-inflammatory drug Montelukast (sold under the brand name Singulair[®]) of the leukotriene receptor antagonist (LTRA) family. LTAs have bronchodilatory and anti-inflammatory effects, typically used together with inhaled corticosteroids in the maintenance treatment of adult and pediatric asthma.⁶² We injected culture medium supplemented with Montelukast (0.006 µg/ml) into models for 2 h prior to cellular exposure at the ALI to either ventilation or control conditions. The models were subsequently analyzed for cell death (i.e., apoptosis/necrosis) and cytokine secretions (i.e., IL-6, IL-8 and IL-10) following the previous section's protocol. Figure 5a-c plots cell cytometry analysis following apoptosis/necrosis staining 24 h following the ventilation/control exposure, identified previously as a critical time point in developing a biotraumatic response. In Figure 5a, we report a significant increase (55%) in the total percentage of live cells analyzed from ventilated models treated prophylactically with Montelukast relative to models ventilated with no prior treatment. The increase of live cells in the prophylactically treated, ventilated group follows the reduction (75%) in apoptotic cells (Figure 5b) in this same group. Though the percent population of necrotic cells in all groups was small (1%–5%), as shown in Figure 5c, we measured a significant increase (70%) in necrotic cells in the Montelukast treated, ventilated group. We found no significant change due to prophylactic treatment in either control group, with viable cell count measured >95% in all nonventilated models.

In Figure 5d-f, we report the effect of prophylactic Montelukast treatment on epithelial cell cytokine secretions. In the ventilated group, where we previously measured a reduction in pro-inflammatory IL-6 and IL-8 following ventilation exposure, we see a similar reduction (Figure 5a,b) although values of IL-6 are significantly higher (67%) in the pre-treated group relative to nontreated. We note that while IL-8 secretory levels were unchanged in the ventilated group following prophylactic treatment, a reduction of 50% was measured in the control (i.e., no ventilation exposure) group. Here, we may speculate that Montelukast acts to inhibit IL-8 in respiratory epithelial cells, as similarly reported in a previous review on the anti-inflammatory activities of β2-agonists.⁶³ For IL-10 (Figure 5f), we

measure a reduction (30%) to near-baseline levels in the prophylactically treated ventilated models, a reversal relative to the nontreated exposure group. These results suggest that the inflammatory response elicited in our models by ventilation exposure is directly modulated by prophylactic treatment using Montelukast.

3 | DISCUSSION AND CONCLUSION

This study aimed to shed light on the physical pathways contributing to biotrauma; the type of VILI most poorly defined and understood.⁴ Preterm infants are particularly susceptible to extended periods of ventilatory support; the more immature the newborn is at birth the longer the likely period of ventilation and thus the increased risk of respiratory distress severity.⁶⁴ Moreover, preterm infants are considered more susceptible to external stressors as their respiratory organs are not fully matured and functional.⁶⁴ Due to their prolonged exposure to ventilation and their anatomical scales, we based our in vitro airway model on the true-scale anatomy of preterm infants undergoing invasive ventilation. Unlike adult patients suffering from lung disease, the preterm infants' central condition lies in their underdeveloped lungs typically excluding other morbidity, thereby isolating the effects of ventilation from the other underlying conditions such as smoking and diabetes, common among adult ventilated patients.⁶⁴

Following a recent theoretical and computational analysis,³⁰ we hypothesized that flow-induced shear stresses in the tracheobronchial tree's upper regions could be associated with a biotraumatic injury. We designed and constructed a 3D tracheobronchial airway model featuring a fully confluent cultured epithelial cell monolayer. We exposed our model to physiologically relevant ventilation flow conditions and used quantitative fluid dynamics tools to identify the localized airway "hot spots" most susceptible to stress-related injury under intubated mechanical ventilation. We found evidence of epithelium structural destruction (i.e., cell erosion) localized at the impaction site between a flow jet emanating from the ETT tip and the main carina. Advanced in vitro platforms have introduced new bioengineering methodologies to explore human diseases in vitro by recapitulating key physiological functions in isolation, thereby offering new insights that are often well beyond reach in vastly more complex in vivo models.¹⁸ For example, lung-on-chips^{20,65} have established an attractive strategy to study among other human lung inflammation and drug responses in vitro by recreating a human-relevant alveolar microenvironment. To date, some studies have investigated VILI and modeled the downstream barotrauma effects of pressure and membranal stretching at the acinar microscales only,^{43,57,66} whereas convective flow phenomena occurring upstream at the macroscale (i.e., conducting airways) have been largely overlooked.⁶⁷ Yet, upper airway flow phenomena drive downstream effects and thereby influence whole-organ lung function. For VILI studies, omitting the lung macroscale potentially implies overlooking the primary insult's origin, namely, where the invasive medical intervention at the root of the problem first meets the patient. A gap thus exists between macroscale

physiological flow phenomena characteristic of actual clinical settings and the downstream flow conditions introduced in microscale in vitro models, where mechanotransduction signaling pathways have been identified.⁶⁸ Here, our hypothesis for flow-induced biotrauma is rooted in the fluid dynamics of the clinical environment and the derivative shear forces imposed on the macro architecture of the upper airways.

We sought a simple and robust in vitro model for exploring the intubated ventilation jet's interaction with the upper airway's epithelium. Extrapolating our computational data and comparing it to other studies that included a broader anatomical scope found that the flow jet's effect is negligible beyond the first several airway generations. Therefore, we designed a model that included the trachea and first three bronchial generations, a relatively limited section of the full respiratory tract. Our flow physics analysis confirmed that the jet's effect is mostly dissipated upon entrance into the second generation in our model due to energy losses beyond the first bifurcations. To explore the cellular response to the introduced flow phenomena, we used our reconstructed airway model's PDMS surface as a scaffold for culturing a monolayer of bronchial epithelial cells, covering the entire three-dimensional lumen. We chose Calu-3, a well-established lung cell line for preclinical pulmonary research that grows confluent layers in immersed conditions and forms barrier junctions. Previous lung-on-chip models have recapitulated other essential aspects of epithelial cell function such as ciliation⁶⁹ and mucus⁴³ secretion by culturing primary cells at an ALI, but have excluded physiologically relevant flow conditions critical to our study. Mucus is an aqueous secretion that offers a critical protective lining to epithelial cells covering the in vivo airways and serves to clear contaminants upward via ciliary motion. While intubated, however, ventilated patients are typically suctioned of secretions,⁷⁰ including mucus, to quickly clear the airways and facilitate breathing. Following clinical guidelines,⁷⁰ our ventilated model similarly excludes mucus, although its potential for protecting against the injury we have identified here warrants further research.

To isolate the effects of mechanical stress from intubated ventilation, we exposed our models to 4 h of clinical ventilation conditions in air; a duration that was short enough to avoid introducing interference owing to the removal of cells from maintenance conditions, that is, immersion in culture medium but sufficiently long to observe a clear cellular response. Furthermore, a 4-h exposure protocol follows previous studies investigating intubated ventilation in "one hit" in vivo^{15,71} and in vitro models,⁷² facilitating the interpretation of our results relative to the broader literature. In the clinical setting, patients can be supported by a ventilator for days or even weeks, likely amplifying the effects measured in our in vitro models following exposure to 4 h alone. In analyzing our models following exposure to ventilated conditions, we first explored changes to the epithelium layer's structural integrity. We found evidence of cell denudation localized primarily at the main carina, matching our flow analysis that identified concentrated levels of high shear stress at the same site, at maximum during the inhalation phase of simulated ventilation. The deleterious effects of a jet stream in the tracheobronchial region were first suspected in the context of high-frequency jet ventilation (HFJV); a

strategy of delivering short pulses of pressurized gas directly into the upper airway through a custom-designed endotracheal lumen. Proposed initially to improve gas exchange and thereby reduce the severity of VILI in both infants⁷³ and adults,⁷⁴ HFJV is no longer recommended for use following a meta-analysis that failed to find an advantage in reducing mortality rates,⁷⁵ in addition to clinical³³ and animal³⁴ studies revealing acute adverse effects (e.g., necrotizing bronchitis, epithelial erosion, loss of surface cilia, and other markers of inflammation). Limitations in trial design and imprecision due to the small number of infants available for these clinical studies increases the possibility that the damaging effects of a jet stream during mechanical ventilation is not restricted to HFJV but could instead apply to all intubated ventilation protocols and not fully appreciated until now.

Previous studies may have also overlooked the potentially harmful effect of intubated flows due to differences in anatomy between humans and laboratory animal species. Rodents have monopodial airway branching, in contrast to the regular dichotomous branching in humans.⁷⁶ This situation likely alters the WSS distribution from intubated ventilation though the effects of these anatomical variations on airflow and have not explicitly been explored. Even within humans, differences in anatomy and airflows exist between pediatric and adult populations, a topic of renewed interest, particularly in pharmacological dosing of respiratory drugs.⁵⁰ Here, we found that epithelial erosion exhibited 48 h after the 4-h ventilation exposure in our simplified, symmetrically bifurcating airway model. While a lengthier exposure may have incurred more extensive damage, the delayed occurrence of cell structural destruction indicates that the ventilation jet's most immediate impact within such timeframe is likely to be a more subtle and complex biological response rather than a singular, acute phenomenon.

To further explore the cellular response in our model and the possible development of biotrauma following invasive ventilation, we measured cell death (apoptosis/necrosis assay) and cytokine secretions. Models were analyzed at 24 and 48 h following exposure, with viability in the ventilated group reduced by 60%, with more than half to apoptosis, while the controls retained over 95% live cells. Measurement of cytokines secreted in the culture medium revealed increased secretion of an anti-inflammatory mediator (IL-10) while simultaneously measuring reduced secretions of pro-inflammatory IL-6 and IL-8 linked to ventilation exposure.^{46,61} Owing to its anti-inflammatory effects, IL-10 has been proposed as a potential therapeutic after showing protective benefit in mice given nebulized IL-10 before injurious ventilation.¹⁵ Mechanical ventilation is generally considered inflammation promoting, with different strategies eliciting different inflammatory responses measured by increased production of cytokines TNF- α , IL-1 β , IL-6, and IL-8.⁷⁷ Interpreting our cytokine measurements could indicate the beginning of a healing process⁵⁶ within our model following a 4-h exposure period, though the role of mediators involved in respiratory inflammation and VILI remains controversial owing to inconsistent results.¹⁵ In a rat model of acute respiratory distress syndrome (ARDS), Chiumello et al.¹⁴ showed that local and systemic pro-inflammatory cytokines increase over time

after the beginning of injurious ventilation, with a high peak between 2 and 4 h. In a human randomized control trial, however, concentrations of IL-6 and IL-8 in bronchoalveolar lavage fluid and blood serum samples from ventilated ARDS patients showed differences 36–40 h following ventilation, whereas levels remained close to baseline when measured between 24 and 30 h after ventilation. While we found that changes in cytokines were most significant at 24 h following ventilation, it is difficult to extrapolate our results directly to a clinical insight in either infant or adult patients. However, the mechanical damage exhibited only 48 h after the ventilation exposure suggests a much more subtle form of biological damage, tying into the hypothesis of biotrauma related to VILI.

To establish a proof-of-concept for our model's application as a preclinical in vitro platform for drug screening, we tested our system's response to Montelukast (Singulair[®]), an anti-inflammatory LTRA commonly used via oral formulation in treating or preventing bronchial asthma among pediatric and adult patients.⁶² In preterm infants, corticosteroids are still the mainstay for immunosuppression, proven to improve short-term lung function. However, newly uncovered adverse effects on neurological development^{78,79} have led to the search for steroid-sparing solutions to treat inflammation in this vulnerable population. Direct topical drug delivery has the advantage of significant efficacy at the anatomical site of interest while avoiding potential drug-related adverse events which may develop following the systemic administration of formulations. Montelukast's potential for reducing inflammation among premature infants would carry significant clinical value. The prophylactic topical delivery of Montelukast in our models demonstrates that the cellular and inflammatory response induced by exposure to clinical ventilation conditions could be modulated pharmacologically. In models pre-treated with Montelukast and subsequently exposed to injurious ventilation, we found increased cell viability together with changes to cytokine secretions, aligning with clinical outcomes found in vivo.^{80–82} While further experiments are necessary to investigate the longer-term effects of this intervention, these findings demonstrate the in vitro platform's potential as a lung biotrauma model and a potent preclinical tool for identifying new therapeutic opportunities. Our efforts support recent calls to advance the development of human-relevant preclinical in vitro models in light of the ongoing lack of effective therapeutic treatments of lung diseases.⁸³

4 | METHODS

4.1 | Model fabrication

Fabrication of the neonatal tracheobronchial model (Figure 1a) begins with the computer-aided design (CAD) of a planar, symmetric double-bifurcating geometry with a constant bifurcating angle of 60°, as schematically shown in Figure 1b. A stereo-lithography type 3D printer (Form3, Formlabs) was used to create a casting template (Figure 1c) in the CAD model's shape shown in Figure 1b. Printing with a layer thickness of 25 μm ensured a smooth surface and fully resolved

details, yielding a total printing time of 24 h. Following postprinting preparation (removal of supports and excess print material), liquid-form PDMS (Sylgard184, Dow Corning) was poured into the cast following the manufacturer's instructions and left to polymerize at room temperature for 24 h. The 3D-printed cast was subsequently dissolved by immersion in acetone for 24 h, leaving a transparent hollow phantom (Figure 1d). More details can be found in a previous study using similar silicone phantom fabrication methods.³⁰ Following the complete dissolution of the last remaining printed material, the PDMS scaffold was left to dry in a well-ventilated space (i.e., chemical hood) for >72 h. PDMS material swells during immersed conditions in acetone, an effect reversed with sufficient drying time. Furthermore, we found that acetone's inadequate evaporation due to shorter drying periods disrupted later cell growth and prevented full monolayer confluence.

4.2 | Model coating

Twenty-four hours before cell seeding, the inner surface of the PDMS phantom models was coated with human plasma fibronectin (#354008) and collagen from bovine skin (#C4243, Sigma-Aldrich) following a coating study for optimal growing conditions of Calu-3 directly on PDMS surfaces (see Figure S1). To coax cells to grow directly on PDMS, we conducted a coating comparison study between cells growing in a 24-well plate. We took bright-field microscopy images of the wells 3-, 5-, and 7-days following cell seeding on three different coatings: 10% fetal bovine serum (FBS), 1% v/v collagen, and a combination of 1% v/v collagen, 1% v/v fibronectin in addition to no coating. The combined fibronectin and collagen coating was found to support full confluence consistently following 7 days and was subsequently used in all models.

4.3 | Cell culture and seeding

Human airway epithelial cell line Calu-3 (American Type Culture Collection) was used in this study (passage number 15–20). Cells were maintained in minimum essential medium-eagle (#01-025-1B, Biological Industries) supplemented with 10% FBS, L-glutamine (#41-218-100, Biological Industries), and 1% antibiotic antimycotic (Sigma-Aldrich, A5955). Calu-3 cells were seeded (10^6 cells) in 180 cm^2 flasks under immersed conditions and reached ~80% confluence after 10 days under standard culture conditions (37°C , 5% CO₂-95% air). Next, $3-4 \times 10^6$ cells (in 250-μl medium) were seeded inside the model. Models were then attached to a rotator (Intelli-Mixer RM-2, ELMI Ltd.) overnight at 1 RPM and subsequently left under immersed conditions and reached 100% confluence after 3–4 weeks. In total, each in vitro model requires approximately one month to transform from a 3D-printed cast to a fully confluent airway lumen. Mycoplasma controls were performed routinely and never showed infection. We note here that selecting a pediatric in vitro model lies within the experimental limitations of culturing an epithelium in a real-scale, full-

sized upper airway geometry; this would not be easily feasible with a full-sized adult airway geometry requiring special incubation space and tremendous efforts to achieve full epithelial coverage.

4.4 | Simulated ventilation experimental setup

An infant-pediatric ventilator (CrossVent2, Bio-Med Devices) was used to ventilate the in vitro model with medical-grade air via a standard neonatal breathing circuit and a 3.0-mm ID ETT (#70-100-111 Blue Line Oral Nasal Endotracheal tube, Smiths Medical). Simulating the function of a compliant lung in the absence of all ~23 generations of airways was achieved by attaching tiny biocompatible water balloons (#FBA-WB-100, Wet Products, Inc.) to the four outlets of the model and secured in place using a plastic adapter (#FCFM-001, Nordson Medical) and thread seal tape. The ventilator maintains a set pressure by adjusting the flow in a closed control feedback loop. Built-in alarm systems on the ventilator and incubator ensured consistent ventilation and environmental conditions for the ventilation exposure duration.

4.5 | Tomographic particle image velocimetry

To perform particle image velocimetry (PIV), one of the most critical requirements is that tracer particles faithfully follow the streamlines of the flow. This requirement is most often met by calculating the Stokes number, which relates the settling time of the particle to the characteristic time of the flow and ensuring it is sufficiently small, that is, $\text{Stk} < 1$. To seed air and most other gases, this would require particle sizes too small to be adequately imaged in the context of our model. As typical to fluid dynamics flow visualization studies, we used instead a glycerol/water solution (58% glycerol by mass) as the working fluid affording increased density and viscosity, thereby allowing 10 μm diameter particles (PSFluoRed; microParticles GmbH) for clear optical imaging and fluorescent reflection. Conversion of experimentally measured values to their air equivalent is straightforwardly done following dimensional analysis, a standard tool in fluid dynamics to relate flow phenomena between different length scales and material properties. In facilitating the visualization experiment and preventing leaks, the ETT was replaced with a nylon tube-to-tube connector (MLSL035-1, Nordson Medical) with similar dimensions but with added lips for securing tubing and placement in the model. A linear motor (PS01-23x160H-HP-R; Linmot) was used to ventilate the upper airway model using a setup described in our previous study³⁰ spanning tidal volumes between 0.5 and 2.5 ml.

4.6 | Numerical methods

The system of governing equations (i.e., conservation of mass and momentum) is solved numerically using a commercial software's FVM (ANSYS Fluent v19.2). The momentum equations are discretized using the second-order upwind scheme for velocity and second-order scheme for

pressure, whereas, for coupling the velocity and pressure fields, the Coupled algorithm is applied along with a least-squares-based scheme for gradients. For numerical modeling purposes, the mouth opening is treated as a velocity inlet, and two bifurcation exits as pressure outlets. Cyclic flow conditions following a sinusoidal velocity profile were applied at the inlet as defined in Figure 2a, matching the flow rate (~ 9.5 ml/s) measured via tomographic PIV at the inlet to the phantom model. The double-bifurcating airway model, including the intubation tube, was meshed with tetrahedral cells using a commercial meshing software (ANSYS ICEM). Rigorous mesh convergence tests were first performed to select the optimal numerical setup ranging from 2.8 to 7.4 M. The final mesh selected for all the numerical simulations is of 4.3 M tetrahedral mesh converted to a polyhedral mesh with 0.74 M cells approximately in Fluent (see Figure S5a). The time step chosen for each scenario was $T/500$, adequately capturing the velocities (Figure S5b,c) present in the range of the simulated ventilation profiles. Note that in matching the TPIV experiments, working fluid of glycerol/water at 58:42 ratio was used for defining the material density and viscosity at room temperature (25°C).

4.7 | Biochemical and cytological analyses

Cytokine levels in sampled medium supernatants were measured using commercially available ELISA kits in a blinded fashion and by following the manufacturer's directions (Invitrogen) for the following cytokines: IL-6 (#88-7066-77), IL-8 (#88-8086-77), and IL-10 (#88-7106-88). For flow cytometry, cells were dissociated from the lumen of the model by adding Trypsin EDTA Solution B (0.25%), EDTA (0.05%) (Biological Industries). Following collection, culture medium (see culture) was added at a 1:1 ratio to block the Trypsin-B effect. Cells were subsequently centrifuged at 3.0 rpm for 3 min., the supernatant discarded and then resuspended in 500 µl of binding buffer, stained with 10 µl of AnnexinV-FITC and PI following manufacturer's instructions (Annexin-V Apoptosis Staining Detection Kit, ab14084, Abcam). Metabolic activity tests were performed using an alamarBlue cell viability assay (BUF012, Bio-rad). The absorbance of the incubated media containing 10% alamarBlue (2 h) was measured at 570 and 600 nm using a microplate reader (Synergy H1, BioTek).

4.8 | Prophylactic medication preparation

Montelukast sodium hydrate (#SML0101, Sigma-Aldrich) was diluted in DMSO to a stock concentration of 0.006 mg/ml and stored in -20°C. Before a prophylactic ventilation experiment, the stock working concentration was further diluted in a culture medium (MEM-eagle) at 1:1000 before injection into the models (0.006 µg/ml).

4.9 | Statistical analyses

Data are presented as the mean with error bars showing the standard deviation (SD). Statistical analyses were performed using Prism 8.0

GraphPad software (GraphPad). Data were analyzed using a un/paired two-sided Student's t-test, One-Way analysis of variance (ANOVA) with Holm-Sidak's post-test, Two-Way ANOVA with Sidak's multiple comparisons test, or as indicated in figure legends. p -values <0.05 were considered statistically significant and are reported in figures using the following notation: * $p < 0.05$; ** $p < 0.01$; *** $p < 0.001$; **** $p < 0.0001$ (with * referring to the comparisons specified in each figure legend).

ACKNOWLEDGMENTS

This work was supported by the European Research Council (ERC) under the European Union's Horizon 2020 research and innovation program (grant agreement no. 677772). We thank Enas Abu-Shah for numerous discussions and critical reading of the manuscript. We thank Karin Gefen-Magiura for important logistical support during unique challenges of the pandemic.

AUTHOR CONTRIBUTIONS

Eliram Nof: Conceptualization (lead); data curation (lead); formal analysis (lead); investigation (lead); methodology (lead); project administration (lead); software (lead); visualization (lead); writing – original draft preparation (lead); writing - review & editing (lead). **Arbel Artzy-Schnirman:** Conceptualization (supporting); investigation (supporting); methodology (supporting); supervision (supporting); validation (supporting); writing - review & editing (supporting). **Saurabh Bhardwaj:** Software (supporting). **Hadas Sabatan:** Investigation (supporting); methodology (supporting). **Dan Waisman** Discussed results; reviewed manuscript. **Ori Hochwald** Discussed results; reviewed manuscript. **Maayan Gruber** Discussed results; reviewed manuscript. **Liron Borenstein-Levin:** Methodology (supporting); resources (supporting). **Josué Sznitman:** Conceptualization (supporting); funding acquisition (lead); resources (lead); supervision (lead); writing - review & editing (supporting).

CONFLICT OF INTERESTS

The authors declare no conflict of interest.

PEER REVIEW

The peer review history for this article is available at <https://publons.com/publon/10.1002/btm2.10271>.

DATA AVAILABILITY STATEMENT

The data that supports the findings of this study are available in the supplementary material of this article.

ORCID

Eliram Nof  <https://orcid.org/0000-0001-6452-1401>

Arbel Artzy-Schnirman  <https://orcid.org/0000-0002-2173-7410>

Saurabh Bhardwaj  <https://orcid.org/0000-0003-3720-9580>

Dan Waisman  <https://orcid.org/0000-0002-6768-0042>

Ori Hochwald  <https://orcid.org/0000-0001-9830-7278>

Liron Borenstein-Levin  <https://orcid.org/0000-0002-9949-4308>

Josué Sznitman  <https://orcid.org/0000-0001-8217-3842>

REFERENCES

1. Wunsch H, Linde-Zwirble WT, Angus DC, Hartman ME, Milbrandt EB, Kahn JM. The epidemiology of mechanical ventilation use in the United States. *Crit Care Med.* 2010;38(10):1947-1953.
2. Slutsky AS. Ventilator-induced lung injury: from barotrauma to biotrauma. *Respir Care.* 2005;50(5):646-659.
3. dos Santos CC, Slutsky AS. The contribution of biophysical lung injury to the development of biotrauma. *Annu Rev Physiol.* 2006;68: 585-618.
4. Curley GF, Laffey JG, Zhang H, Slutsky AS. Biotrauma and ventilator-induced lung injury. *Chest.* 2016;150(5):1109-1117.
5. Marini JJ, Gattinoni L. Management of COVID-19 respiratory distress. *JAMA.* 2020;323(22):2329-2330.
6. Patel BK, Kress JP, Hall JB. Alternatives to invasive ventilation in the COVID-19 pandemic. *JAMA.* 2020;324(1):43-44.
7. Tobin MJ, Laghi F, Jubran A. Caution about early intubation and mechanical ventilation in COVID-19. *Ann Intensive Care.* 2020; 10(1):1.
8. Zhou F, Yu T, Du R, et al. Clinical course and risk factors for mortality of adult inpatients with COVID-19 in Wuhan, China: a retrospective cohort study. *The Lancet.* 2020;395:10229-11062.
9. Auld SC, Caridi-Scheible M, Blum JM, et al. ICU and ventilator mortality among critically ill adults with coronavirus disease 2019. *Crit Care Med.* 2020;48:9-e804.
10. Slutsky AS, Ranieri VM. Ventilator-induced lung injury. *N Eng J Med.* 2013;369(22):2126-2136.
11. Network ARDS. Ventilation with lower tidal volumes as compared with traditional tidal volumes for acute lung injury and the acute respiratory distress syndrome. *N Eng J Med.* 2000;342(18):1301-1308.
12. Matthay MA, McAuley DF, Ware LB. Clinical trials in acute respiratory distress syndrome: challenges and opportunities. *Lancet Respir Med.* 2017;5(6):524-534.
13. Bobba CM, Fei Q, Shukla V, et al. Nanoparticle delivery of microRNA-146a regulates mechanotransduction in lung macrophages and mitigates injury during mechanical ventilation. *Nat Commun.* 2021; 12(1):289.
14. Chiumello D, Pristine G, Slutsky AS. Mechanical ventilation affects local and systemic cytokines in an animal model of acute respiratory distress syndrome. *Am J Respir Crit Care Med.* 1999;160(1):109-116.
15. Hoegl S, Boost KA, Czerwonka H, et al. Inhaled IL-10 reduces biotrauma and mortality in a model of ventilator-induced lung injury. *Respir Med.* 2009;103(3):463-470.
16. Ranieri VM, Suter PM, Tortorella C, et al. Effect of mechanical ventilation on inflammatory mediators in patients with acute respiratory distress syndrome. *JAMA.* 1999;282(1):54-61.
17. Plötz FB, Slutsky AS, Van Vugt AJ, Heijnen CJ. Ventilator-induced lung injury and multiple system organ failure: a critical review of facts and hypotheses. *Intensive Care Med.* 2004;30(10):1865-1872.
18. Benam KH, Dauth S, Hassell B, et al. Engineered In vitro disease models. *Annu Rev Pathol Mech Dis.* 2015;10(1):195-262.
19. Artzy-Schnirman A, Lehr C-M, Sznitman J. Advancing humanin vitro pulmonary disease models in preclinical research: opportunities for lung-on-chips. *Expert Opin Drug Deliv.* 2020;17(5): 621-625.
20. Huh D, Leslie DC, Matthews BD, et al. A human disease model of drug toxicity-induced pulmonary edema in a lung-on-a-chip microdevice. *Sci Transl Med.* 2012;4:159.
21. Felder M, Trueeb B, Stucki AO, et al. Impaired wound healing of alveolar lung epithelial cells in a breathing lung-on-a-chip. *Front Bioeng Biotechnol.* 2019;7:3.
22. Doryab A, Taskin MB, Stahlhut P, et al. A bioinspired in vitro lung model to study particokinetics of nano-/microparticles under cyclic stretch and air-liquid interface conditions. *Front Bioeng Biotechnol.* 2021;9:42.
23. Thompson CL, Fu S, Knight MM, Thorpe SD. Mechanical stimulation: a crucial element of organ-on-chip models. *Front Bioeng Biotechnol.* 2020;8:1426.
24. Tenenbaum-Katan J, Artzy-Schnirman A, Fishler R, Korin N, Sznitman J. Biomimetics of the pulmonary environment in vitro: a microfluidics perspective. *Biomicrofluidics.* 2018;12(4):42209.
25. Jamaati H, Nazari M, Daroeei R, Ghafari T, Raoufy MR. Role of shear stress in ventilator-induced lung injury. *Lancet Respir Med.* 2016;4(8): e41-e42.
26. Neto AS, Hemmes SNT, Barbas CSV, et al. Association between driving pressure and development of postoperative pulmonary complications in patients undergoing mechanical ventilation for general anaesthesia: a meta-analysis of individual patient data. *The Lancet Respir Med.* 2016;4(4):272-280.
27. Chowdhary R, Singh V, Tattersfield AE, Sharma SD, Kar S, Gupta AB. Relationship of flow and cross-sectional area to frictional stress in airway models of asthma. *J Asthma.* 1999;36(5):419-426.
28. Green A. Modelling of peak-flow wall shear stress in major airways of the lung. *J Biomech.* 2004;37(5):661-667.
29. Alzahrany M, Banerjee A, Salzman G. Flow transport and gas mixing during invasive high frequency oscillatory ventilation. *Med Eng Phys.* 2014;36(6):647-658.
30. Nof E, Heller-Algazi M, Coletti F, Waisman D, Sznitman J. Ventilation-induced jet suggests biotrauma in reconstructed airways of the intubated neonate. *J R Soc Interf.* 2020;17(162):20190516.
31. Nucci G, Suki B, Lutchen K. Modeling airflow-related shear stress during heterogeneous constriction and mechanical ventilation. *J Appl Physiol.* 2003;95(1):348-356.
32. Weiner G, Zaichkin J, Kattwinkel J. *Textbook of Neonatal Resuscitation (NRP).* American Academy of Pediatrics; 2016.
33. Boros SJ, Mammel MC, Lewallen PK, Coleman JM, Gordon MJ, Ophoven J. Necrotizing tracheobronchitis: A complication of high-frequency ventilation. *J Pediatr.* 1986;109(1):95-100.
34. Ophoven JP, Mammel MC, Gordon MJ, Boros SJ. Tracheobronchial histopathology associated with high-frequency jet ventilation. *Crit Care Med.* 1984;12(9):829-832.
35. Weibel ER. *Morphometry of the Human Lung.* Springer-Verlag; 1963.
36. Comer JK, Kleinstreuer C, Zhang Z. Flow structures and particle deposition patterns in double-bifurcation airway models. Part 1. Air flow fields. *J Fluid Mech.* 2001;435:25-54.
37. Jalal S, Van de Moortele T, Nemes A, Amili O, Coletti F. Three-dimensional steady and oscillatory flow in a double bifurcation airway model. *Phys Rev Fluids.* 2018;3:103101.
38. Bauer K, Nof E, Sznitman J. Revisiting high-frequency oscillatory ventilation in vitro and in silico in neonatal conductive airways. *Clin Biomech.* 2019;66:50-59.
39. Foster KA, Avery ML, Yazdanian M, Audus KL. Characterization of the Calu-3 cell line as a tool to screen pulmonary drug delivery. *Int J Pharm.* 2000;208(1-2):1-11.
40. Kreft ME, Jerman UD, Lasić E, et al. The characterization of the human cell line Calu-3 under different culture conditions and its use as an optimized in vitro model to investigate bronchial epithelial function. *Eur J Pharm Sci.* 2015;69:1-9.
41. Ehrhardt C, Forbes B, Kim K-J. *In Vitro Models of the Tracheo-Bronchial Epithelium,* 235-257. Springer; 2008.
42. Bischel LL, Sung KE, Jiménez-Torres JA, Mader B, Keely PJ, Beebe DJ. The importance of being a lumen. *FASEB J.* 2014;28(11):4583-4590.
43. Baptista D, Teixeira LM, Birgani ZT, et al. 3D alveolar in vitro model based on epithelialized biomimetically curved culture membranes. *Biomaterials.* 2021;266:120436.
44. Sidhaye VK, Schweitzer KS, Caterina MJ, Shimoda L, King LS. Shear stress regulates aquaporin-5 and airway epithelial barrier function. *Proc Natl Acad Sci U S A.* 2008;105(9):3345-3350.
45. Pedley T. Pulmonary fluid dynamics. *Annu Rev Fluid Mech.* 1977; 9(1):229.

46. Parsons PE, Eisner MD, Thompson BT, et al. Lower tidal volume ventilation and plasma cytokine markers of inflammation in patients with acute lung injury. *Crit Care Med.* 2005;33:1-6.
47. Corrado A, Gorini M, Villegas G, De Paola E. Negative pressure ventilation in the treatment of acute respiratory failure: an old noninvasive technique reconsidered. *Eur Respir J.* 1996;9(7):1531-1544.
48. Sul B, Wallqvist A, Morris MJ, Reifman J, Rakesh V. A computational study of the respiratory airflow characteristics in normal and obstructed human airways. *Comput Biol Med.* 2014;52:130-143.
49. Koombua K, Pidaparti RM. Inhalation induced stresses and flow characteristics in human airways through fluid-structure interaction analysis. *Modelling and Simulation in Engineering.* 2008;2008:358748.
50. Das P, Nof E, Amirav I, Kassinos SC, Sznitman J. Targeting inhaled aerosol delivery to upper airways in children: Insight from computational fluid dynamics (CFD). *PLoS One.* 2018;13(11):e0207711.
51. Muller W, Gerjarusek S, Scherer P. Studies of wall shear and mass transfer in a large scale model of neonatal high-frequency jet ventilation. *Ann Biomed Eng.* 1990;18(1):69-88.
52. Bauer K, Brücker C. The role of ventilation frequency in airway reopening. *J Biomech.* 2009;42(8):1108-1113.
53. Keszler M. Mechanical ventilation strategies. *Semin Fetal Neonatal Med.* 2017;22(4):267-274.
54. Sweet DG, Carnielli V, Greisen G, et al. European consensus guidelines on the management of respiratory distress syndrome – 2019 update. *Neonatology.* 2019;115(4):432-450.
55. Polak MJ, Donnelly WH, Bucciarelli RL. Comparison of airway pathologic lesions after high-frequency jet or conventional ventilation. *Am J Dis Child.* 1989;143(2):228-232.
56. Crosby LM, Waters CM. Epithelial repair mechanisms in the lung. *Am J Physiol Lung Cell Mol Phys Ther.* 2010;298(6):L715-L731.
57. Douville NJ, Zamankhan P, Tung Y-C, et al. Combination of fluid and solid mechanical stresses contribute to cell death and detachment in a microfluidic alveolar model. *Lab Chip.* 2011;11(4):609-619.
58. Drakopanagiotakis F, Xifteri A, Polychronopoulos V, Bouros D. Apoptosis in lung injury and fibrosis. *Eur Respir J.* 2008;32(6):1631-1638.
59. White SR. Apoptosis and the airway epithelium. *J Allergy.* 2011;2011:2011-2021.
60. Haggi M, Young PM, Traini D, Jaiswal R, Gong J, Bebawy M. Time- and passage-dependent characteristics of a Calu-3 respiratory epithelial cell model. *Drug Dev Ind Pharm.* 2010;36(10):1207.
61. Moore KW, de Waal Malefyt R, Coffman RL, O'Garra A. Interleukin-10 and the Interleukin-10 Receptor. *Annu Rev Immunol.* 2001;19(1):683-765.
62. Trinh HKT, Lee S-H, Cao TBT, Park H-S. Asthma pharmacotherapy: an update on leukotriene treatments. *Expert Rev Respir Med.* 2019;13(12):1169-1178.
63. Theron AJ, Steel HC, Tintinger GR, Feldman C, Anderson R. Can the anti-inflammatory activities of β2-agonists be harnessed in the clinical setting? *Drug Des Dev Ther.* 2013;7:1387-1398.
64. Zayegh AM, Davis PG. BPD treatments: The never-ending smorgasbord. *Semin Fetal Neonatal Med.* 2021;26(2):101223. <https://doi.org/10.1016/j.siny.2021.101223>
65. Artzy-Schnirman A, Hobi N, Schneider-Daum N, Guenat OT, Lehr C-M, Sznitman J. Advanced in vitro lung-on-chip platforms for inhalation assays: From prospect to pipeline. *Eur J Pharm Biopharm.* 2019;144:11-17.
66. Bilek AM, Dee KC, Gaver DP III. Mechanisms of surface-tension-induced epithelial cell damage in a model of pulmonary airway reopening. *J Appl Physiol.* 2003;94(2):770-783.
67. Jimenez-Valdes RJ, Can UI, Niemeyer BF, Benam KH. Where we stand: lung organotypic living systems that emulate human-relevant host-environment/pathogen interactions. *Front Bioeng Biotechnol.* 2020;8:989.
68. Ghadiali SN, Gaver DP. 1 232, respiratory biomechanics. *Respir Physiol Neurobiol.* 2008;163:163-243.
69. Elias-Kirma S, Artzy-Schnirman A, Das P, Heller-Algazi M, Korin N, Sznitman J. In situ-like aerosol inhalation exposure for cytotoxicity assessment using airway-on-chips platforms. *Front Bioeng Biotechnol.* 2020;8:91.
70. American Association for Respiratory Care. AARC Clinical Practice Guidelines. Endotracheal suctioning of mechanically ventilated patients with artificial airways 2010. *Respir Care.* 2010;55:758-764.
71. Wong JJM, Lee SW, Tan HL, et al. Lung-protective mechanical ventilation strategies in pediatric acute respiratory distress syndrome. *Pediatr Crit Care Med.* 2020;21(8):720-728.
72. Harris C, Thorpe SD, Rushwan S, et al. An in vitro investigation of the inflammatory response to the strain amplitudes which occur during high frequency oscillation ventilation and conventional mechanical ventilation. *J Biomech.* 2019;88:186-189.
73. Pokora T, Bing D, Mammel M, Boros S. Neonatal high-frequency jet ventilation. *Pediatrics.* 1983;72(1):27-32.
74. Carlon GC, Kahn RC, Howland WS, Cole Ray J, Turnbull AD. Clinical experience with high frequency jet ventilation. *Crit Care Med.* 1981;9(1):1-6.
75. Rojas-Reyes M, Orrego-Rojas P. Rescue high-frequency jet ventilation versus conventional ventilation for severe pulmonary dysfunction in preterm infants. *Cochrane Database Syst Rev.* 2015;10:CD000437.
76. Meyerholz DK, Suarez CJ, Dintzis SM, Frevert CW. Respiratory system. In: Treuting PM, Dintzis SM, Montine KS, eds. *Comparative Anatomy and Histology (Second Edition).* 2nd ed. Academic Press; 2018:147-162.
77. Hong CM, Xu D-Z, Lu Q, et al. Low tidal volume and high positive end-expiratory pressure mechanical ventilation results in increased inflammation and ventilator-associated lung injury in normal lungs. *Anesth Analg.* 2010;110(6):1652-1660.
78. Barrington KJ. The adverse neuro-developmental effects of postnatal steroids in the preterm infant: a systematic review of RCTs. *BMC Pediatr.* 2001;1(1):1.
79. Carson R, Monaghan-Nichols AP, DeFranco DB, Rudine AC. Effects of antenatal glucocorticoids on the developing brain. *Steroids.* 2016;114:25-32.
80. Diamant Z, van der Molen T. Treating asthma: is there a place for leukotriene receptor antagonists? *Respir Med.* 2005;99(6):655-662.
81. Rupprecht T, Rupprecht C, Harms D, Sterlacci W, Vieth M, Seybold K. Leukotriene receptor blockade as a life-saving treatment in severe bronchopulmonary dysplasia. *Respiration.* 2014;88(4):285-290.
82. Chen X, Zhang X, Pan J. Effect of montelukast on bronchopulmonary dysplasia (BPD) and related mechanisms. *Med Sci Monit.* 1886;2019:25-1893.
83. Artzy-Schnirman A, Raviv SA, Fikshtain OD, et al. Advanced human-relevant in vitro pulmonary platforms for respiratory therapeutics. *Adv Drug Deliv Rev.* 2021;176:113901.

SUPPORTING INFORMATION

Additional supporting information may be found in the online version of the article at the publisher's website.

How to cite this article: Nof E, Artzy-Schnirman A, Bhardwaj S, et al. Ventilation-induced epithelial injury drives biological onset of lung trauma in vitro and is mitigated with prophylactic anti-inflammatory therapeutics. *Bioeng Transl Med.* 2021;e10271. doi:10.1002/btm2.10271